

## Application of alteration index and zoning for Pb-Zn exploration in Haft-Savaran area, Khomein, Iran

N. Zandy Ilghani<sup>1</sup>, F. Ghadimi<sup>1\*</sup> and M. Ghomi<sup>1,2</sup>

1. Department of Mining Engineering, Arak University of Technology, Arak, Iran

2. Mining and Metallurgical Engineering Department, Amirkabir University of Technology (Tehran Polytechnic), Tehran, Iran

Received 16 August 2017; received in revised form 23 October 2017; accepted 25 October 2017

\*Corresponding author: [ghadimi@arakut.ac.ir](mailto:ghadimi@arakut.ac.ir) (F. Ghadimi).

### Abstract

The Haft-Savaran Pb-Zn mineralization zone with the lower Jurassic age is located in the southern basin of Arak and Malayer-Isfahan metallogenic belt of Iran. Based upon the geological map of the Haft-Savaran area, the sandstone and shale of lower Jurassic are the main rocks of Pb-Zn deposit. In this area, 170 samples were taken from 33 boreholes, and 44 elements were measured by the ICP-MS method. Adaptation of the alteration index and Pb-Zn mineralization was investigated in this work. The model was created based on the Sericitic, Spitz-Darling, Alkali, Hashimoto, and Silicification Indices in all boreholes. This work showed that the Sericite, Hashimoto, Spitz-Darling, and Silicification indices increased around mineralization, and the alkali index decreased around it. Development of the alteration indices indicates that direction of the ore-bearing solution is NE-SW, and that this trend is consistent with the faults in the area. Based upon the 3D models and other data interpretations, Pb-Zn and elements such as Fe, Mn, Cr, and Ni have deposited within the alteration zones.

**Keywords:** *Alteration Halos, Alteration Index, Pb-Zn Mineralization, Haft-Savaran.*

### 1. Introduction

Iran has large deposits of Pb-Zn (About 600 Pb-Zn deposits and occurrences), among which are the world-class deposits of Mehdiabad, Irankuh, and Angouran [1-3]. Only a few deposits have been actually explored and/or exploited, although 10 deposits are currently being mined [4]. It is probable that those deposits range from exhalative sedimentary to Mississippi Valley-Types (MVTs) [5]. The most important metallogenic provinces for Pb-Zn mineralization are Central Iran, Sanandaj-Sirjan zone, and Alborz region (Figure 1). Ages of the mineralization events and host rocks range from upper Proterozoic to Oligocene-Miocene, although most of the host rocks are either Paleozoic or Cretaceous carbonates [6]. The lead-zinc deposits are common in the Sanandaj-Sirjan zone, especially in its middle part, the Malayer-Esfahan belt, where it is predominantly strata-bound and restricted to Cretaceous limestones, dolomites,

shales, and occasionally sandstones, although some deposits have pre-Cretaceous host rocks. Sulfidic mineralization is dominant in the belt but non-sulfide ores are also common (e.g. Irankuh deposit). The proposed hypothesis for the origin of these deposits vary from MVT to Sedex models [1]. Lead-Zinc deposits are hosted by both clastic and carbonate Phanerozoic rocks. Although many Pb-Zn deposits are Mississippi Valley-type (MVT) [7], the largest deposits (Koushk, Zarigan, and Chahmir) belong to the shale hosted Pb-Zn mineralization type [8]. There are relatively few published data about the Iranian shale-hosted Pb-Zn deposits, and their classification.

A mineral deposit model usually provides systematic descriptions of the essential geological, geophysical, and geochemical characteristics of a relevant type of mineral deposits. The primary geochemical halo of a mineral deposit has been defined originally as an environment including

enriched ore-forming and associated elements, which are formed by hydrothermal ore processing [9-11]. Thus a research work on primary haloes may form part of a mineral deposit model, although both the deposit model and primary halo approaches are based upon the study of primary geochemical features of mineral deposits. These features are the essential mechanisms for metal precipitation or mineral formation, and are indicative of chemical processes that occur during mineralization [12]. The primary geochemical halo is usually applied in mineral exploration of a country or a province, and the results obtained are important for understanding the general distribution of elements. Most studies have focused on deposit-scale exploration programs for primary geochemical haloes in mineral deposits, employing a traditional element zonality method to interpret the litho-geochemical data [13, 14].

Litho-geochemical data are useful for mineral exploration studies by providing chemical information on the alteration and mineralization patterns. The ultimate goal of the statistical and spatial analysis of litho-geochemical data for mineral exploration is the detection of zones of elevated concentrations (e.g. geochemical anomalies) of oxide or trace elements that may be reflective of mineral deposits [15]. One of the major improvements in mineral exploration has been the recognition of regional-scale alteration patterns in hydrothermal systems [16]. Alteration indices allow for more accurate mapping of hydrothermal alteration in rocks, and have been instrumental in the discovery of many base and precious metal ore deposits in both the submarine and sub-aerial environments [17]. One of the questions raised is whether there is a relationship between Pb-Zn mineralization and alteration in the region.

This paper demonstrates the use of regional geochemical surveys for Pb-Zn exploration and local litho-geochemical for mapping alteration intensity at the Haft-Savaran Pb-Zn mineralization.

## 2. Geological setting

The studied area is situated in the Malayer-Esfahan Pb-Zn metallogenic belt within a regional tectono-stratigraphic trend of well-studied nearby Pb-Zn deposits, namely Ahangaran, Emarat, Muchan, Kelisheh, Haft-Savaran, Lakan, Hossein-Abad, which are all of the strata-bound style. From the regional tectonic view point, these deposits are arranged on the margins of a rift-generated sedimentary basin. In places that

intrusive bodies/stocks have outcropped, grade and tonnage of these deposits have considerably improved; however, nearby the Haft-Savaran Pb-Zn deposit, no such outcrops have been observed, requiring airborne magnetic interpretation with adequate line-spacing survey resolution to determine the possibility of hidden intrusive bodies with various magnetic susceptibility and depths in order to estimate their composition [18].

The deposit is situated about 25 km SW of Khomein and SE of Arak city in the Sanandaj-Sirjan zone (Figure 1). A simplified geologic map of the Haft-Savaran region is shown in Figure 2. Based on the geological map of the Haft-Savaran area, sandstone and shale of lower Jurassic are the main rocks in the deposit. Faults with dominant NE-SW trends and folds with S-W or NW-SE trends are the major structural features in the area. In this area, geological formations are comprised of Jurassic (Liassic coal-bearing shale and sandstone) and Cretaceous (limestone).

## 3. Mineralization

The Pb+Zn, Pb/Pb+Zn, Cu+Pb+Zn, and Cu ratios in the shales and sandstone show that mineralization is Sedex deposit in the Haft-Savaran region [18]. Lead-zinc mineralization has occurred in shales and sandstones and along the normal fault with a NE to SW trend. Mineralization is in the form of strata-bound ore deposits. Haft-Savaran deposit is classified into three facies as stockwork, massive sulfide, and stratiform according to geometry, texture, and grade. Mineralization is in form of veins and veinlets in the stockwork facies. Thickness of veins and veinlets change from 1 mm to 4 cm, filled with quartz, dolomite, and sulfide. The thickness and the density veins and veinlets increase in the vicinity of the sulfide massive ore facies. Mineralization includes quartz, iron-rich dolomite, sericite, pyrite, sphalerite, galena, and chalcopyrite. Sulfides are also present in all veins. The grade of Pb-Zn is 5% in stockwork facies. The massive sulfide facies is thick and forms a high-grade deposit in the vicinity of a normal fault above the stockwork facies. Mineralization is strata-bound in the massive sulfide deposit and includes the silica, carbonate, and sericite alterations. Replacement and breccia structure is also seen in this facies due to faulting. Fine-grained sulfides are also observed in sparse in the breccia structure. Massive sulfide facies include dolomite and quartz minerals with sulfides such as pyrite,

sphalerite, galena, and chalcopyrite. The Pb-Zn grade varies from 10 to 18% [18]. Stratiform facies have sulfide strips whose thickness change from 5 mm to 3 cm. This deposit includes silt particles, organic matter, and sulfide minerals. Sulfides are pyrite, and are often dispersed grains. The sphalerite and chalcopyrite minerals are also dispersed in the matrix. The alteration minerals such as fine-grained dolomite and sericite are formed in this facies. The grade of Pb-Zn ore is

very low (0.5%). The shale and sandstone host rock is subjected to silica, dolomite, and sericite hydrothermal alteration, and is mainly found around the stockwork facies. Stockwork sulfide facies and alterations related to the hydrothermal processes and mineralizations have been induced by passing fluids through normal faults in the Haft-Savarar region. A simplified stratigraphic column of the area is shown in Figure 3.

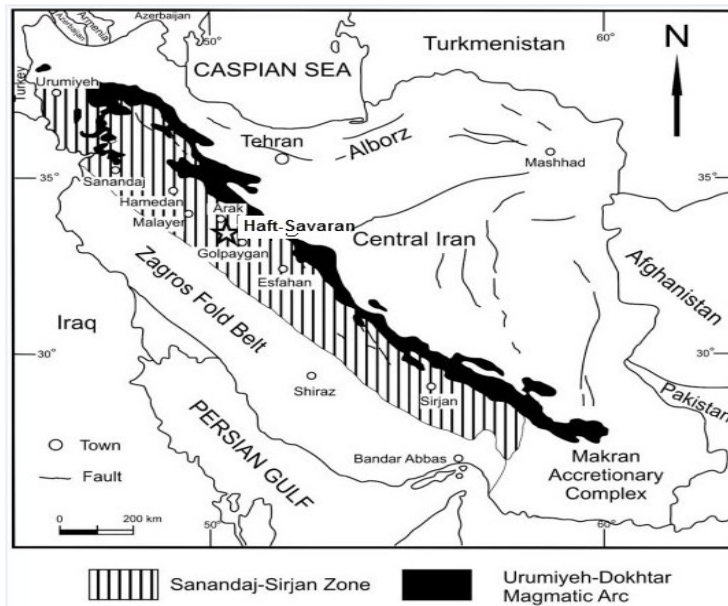


Figure 1. Haft-Savarar Pb-Zn deposit in Sanandaj-Sirjan zone [1].

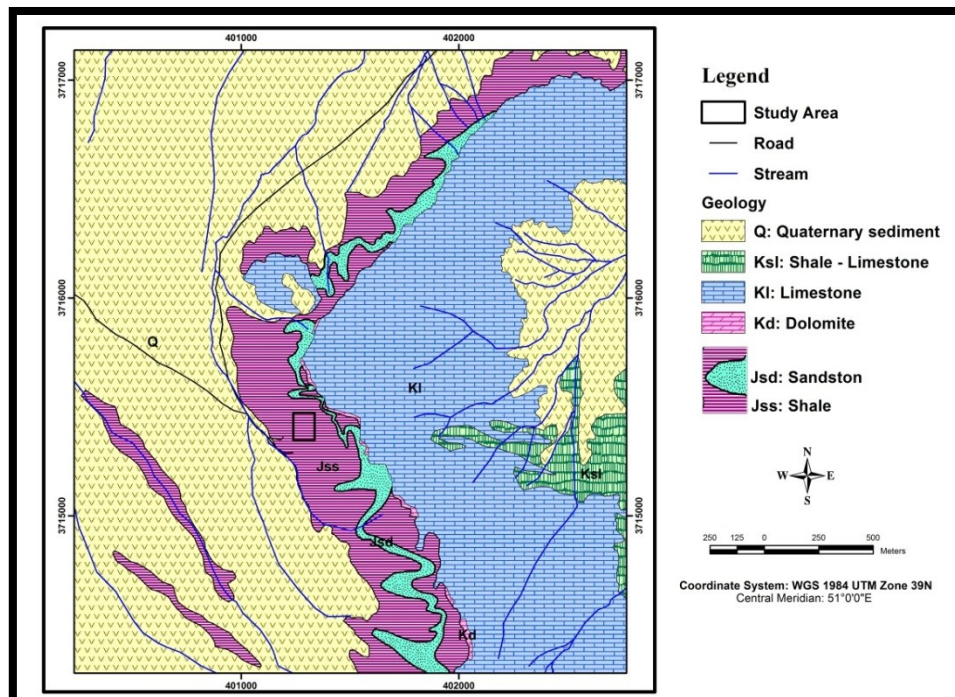


Figure 2. Simplified geologic map of Haft-Savarar region.

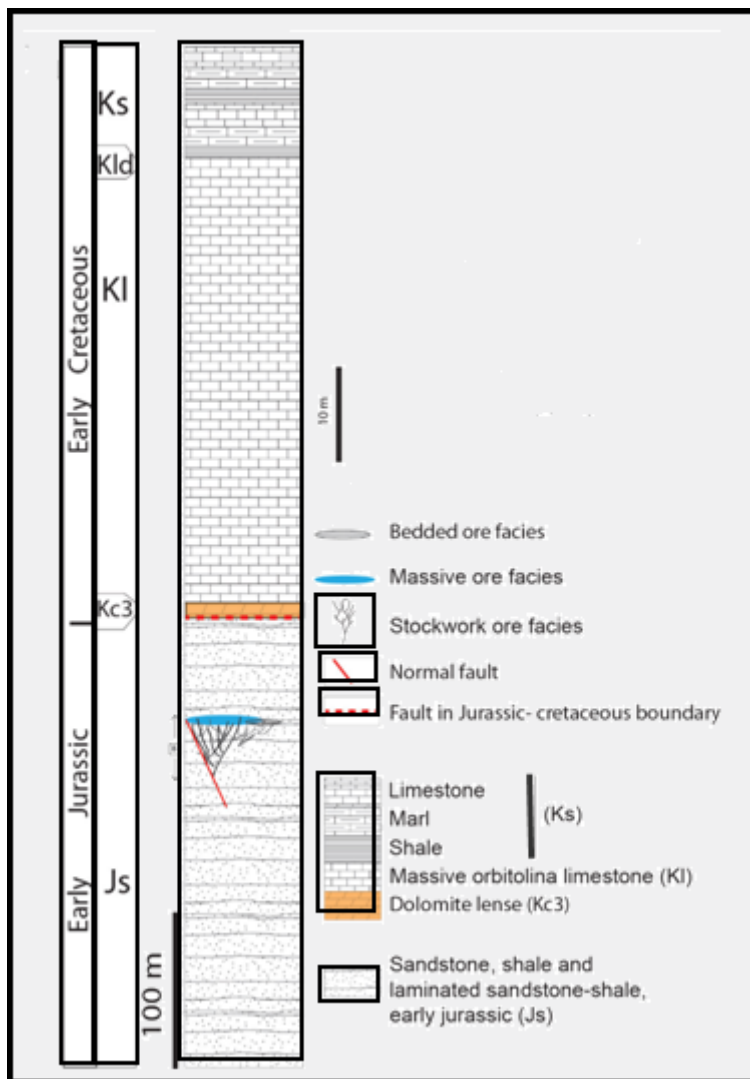


Figure 3. Simplified stratigraphy column of Haft-Savaran deposit [19].

#### 4. Materials and methods

##### 4.1. Sampling and analysis methods

To design the sampling pattern, a total of 33 boreholes with 170 samples were selected from the exploration report for analysis. The location map of boreholes is presented in Figure 4. The samples were analyzed by inductively coupled plasma-mass spectrometry (ICP-MS) for 44 elements (Ag, Al, As, Au, Ba, Be, Bi, Ca, Cd, Ce, Co, Cr, Cs, Cu, Fe, Hg, K, La, Li, Mg, Mn, Mo, Na, Nb, Ni, P, Pb, Rb, Re, S, Sb, Sc, Sn, Sr, Te, Th, Ti, Tl, U, V, W, Y, Zn, and Zr), and major oxides (MgO, Fe<sub>2</sub>O<sub>3</sub>, Al<sub>2</sub>O<sub>3</sub>, Na<sub>2</sub>O, K<sub>2</sub>O, CaO, and SiO<sub>2</sub>) were measured by the X-ray fluorescence (XRF) spectrometer method.

Statistical methods are generally used in analyzing and processing data in geochemical discoveries. The collected data is first organized, and after classification, it is determined out of order data and then normalized data. Finally, the geochemical maps are provided after single-variable and multivariate statistical calculations, and are introduced to the anomalous areas. Accordingly, the goal of geochemical exploration is to obtain geochemical zones using the detector and reagent elements. Therefore, we used different methods of halo indexing and alteration to introduce the mineralization zones. Factor analysis and cluster analysis were used to determine the similarity of different methods of halo index and alteration index.

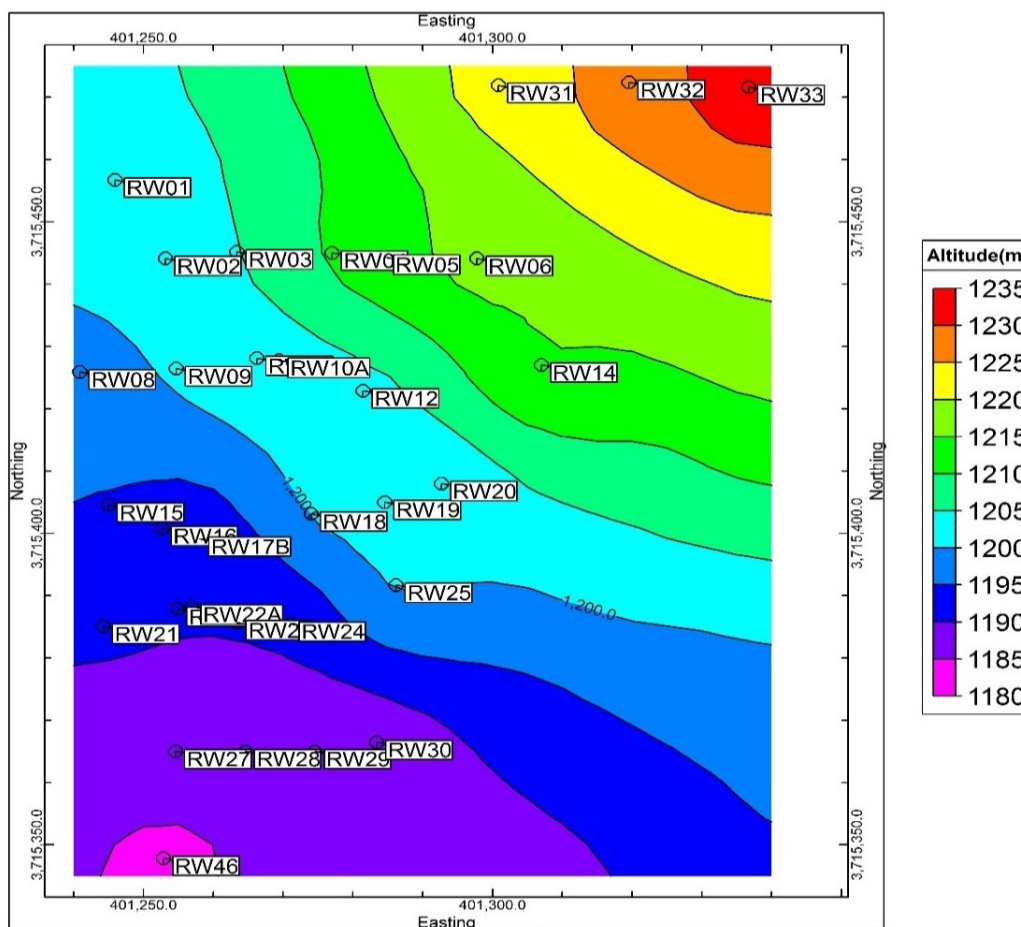


Figure 4. Location map of boreholes.

**4.2. Multivariate analysis**

In order to determine the relationships among the elements, the halo and alteration index groups, factor analysis, and cluster analysis were employed. The results obtained were evaluated by the STATISTICA programs. The factor analysis was carried out by the principal component method, which was, rather than the original data, based upon the examination of dependency among the artificial variables computed from the covariance and correlation coefficient matrices [19]. In other words, the eigenvalues and eigenvectors of covariance and correlation coefficient matrices were interpreted. In the meantime, to strengthen the factor loads, varimax rotation was performed. Using the Ward's method and Pearson's correlation coefficients, cluster analysis (hierarchical cluster analysis) was carried out, and the results obtained were given in a dendrogram.

**5. Results and discussion**

**5.1. Geochemical distribution**

The geochemical characteristics of most important normalized elements are summarized

in appendix 1, with the minimum, maximum, standard deviation, mean, kurtosis, and skewness values. The values for  $X+2S$  ( $X$  is the mean and  $S$  is standard deviation) were calculated for the elements Pb, Zn, Fe, and Cr based on the lepelier method [20]. The Kriging method provided a probability based on estimation of the trace and heavy element distributions and their spatial distributions [21]. It should be noted that Pb and Zn are highly rich in the region (Figure 5). High values of Pb and Zn have a wide distribution in the SW part of the region. The highest values of Fe are located in the SW region with a trend to the NE (Figure 5).

Factor analysis was employed to determine the relationships among the elements and the element groups [22]. Factor analysis yielded five rotated components, each with eigenvalues greater than 1 (Table 1). Twenty three elements were combined and produced five significant factors explaining 71.34% of the variance of the original dataset (Table 1). Most of the variance in the original dataset is contained in factor 1 (32.66%), which is associated with the components

Cr,Zr,Ti,V,Ba,P,Fe, and Pb. Factor2 explains 21.05% of the variance, and is mainly related to the elements Mg,Al,Si,K, and Ca. Ta,Zn,Na, and S contribute most strongly to the third factor that explains 6.76% of the total variance. The fourth factor is concerned with Cr and Cl and represents 6.05% of the total variance. The fifth factor is included solely with Sr, and represents 4.83% of the total variance. There is a good correlation between Pb, Fe, and Cr in factor1 and Zn in factor3 as the mining elements.

Factor analysis allows us to calculate a single value for each factor [23, 24].For example, instead of analyzing separate element maps, we can establish a linear relationship among variables and plot a single map called the factor score (FS) map showing the distribution of such relationship [25, 26].A potential map was obtained by combining the individual FS maps into a single geochemical predictive map, and locations of the studied area were selected as the target areas for further exploration of the deposit-type. After the FSs of each sample, weights should be assigned to each sample to represent the probability of the presence of the deposit-type upstream of the sample. The weights are here called the geochemical mineralization probability index map (GMPI:27, 20).

In general, in a factor analysis, the response variable is continuous, and the values outside the [0, 1] range are inappropriate if the response variable relates to probability. In order to constrain the values of the predicted response variable within the unit interval [0,1], Yousefi et al. [27, 28] and Yousefi and Carranza [28] recommended the use of a logistic model in order to represent the probability, by following:

$$MPI = \frac{e^{FS}}{1 + e^{FS}}$$

where FS is the factor score of each sample per indicator factor obtained in a factor analysis. GMPI is, therefore, a fuzzy weight of each stream sediment geochemical sample for each indicator factor. In this work, the distributions of GMPI for the indicator factors were represented as the interpolated values (Figure 6). A GMPI value corresponding to the cumulative percentile of 97.5% frequency was selected as the threshold value to separate the anomalous and background samples. The map of the first and third geochemical mineralization probability index (GMPI1, GMPI3) shows high values of Pb, Zn, Fe, and Cr in the SW part of the region.

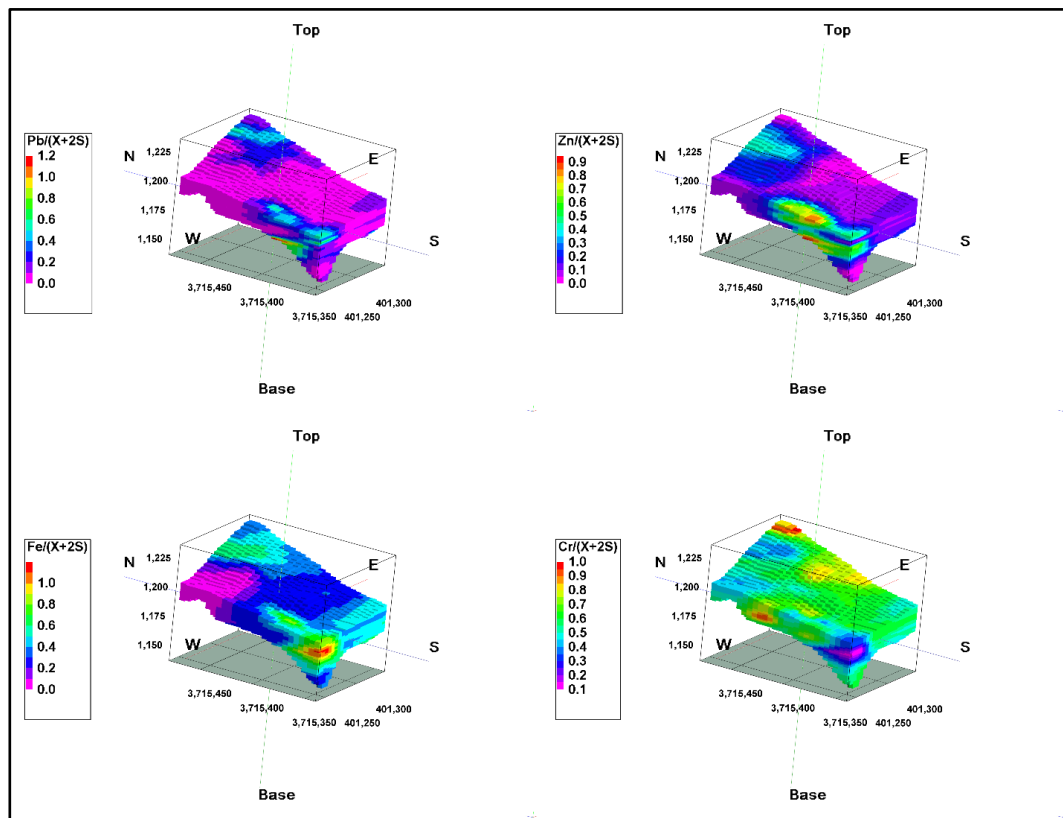


Figure 5. 3D distribution models for elements Pb, Zn, Fe, and Cr.

**Table 1. Factor analysis of elements in first step (loadings in italic represent selected factors based on threshold of 0.70).**

Variables	Factor 1	Factor 2	Factor 3	Factor 4	Factor 5
Cr	-0.65	0.12	-0.10	0.63	0.02
Cu	0.29	0.09	0.47	-0.32	0.10
Fe	0.88	0.02	0.09	0.08	0.12
Mn	0.16	0.48	0.36	0.27	-0.23
Ni	-0.35	-0.01	-0.36	0.04	0.57
Pb	0.64	-0.05	0.46	0.09	0.06
Sr	0.10	-0.21	-0.01	-0.02	0.81
Ta	0.44	-0.14	0.62	-0.12	0.08
Zn	0.20	0.10	0.70	0.12	-0.15
Zr	-0.82	-0.01	-0.02	0.05	-0.24
Ti	-0.93	0.18	-0.13	0.02	0.16
Rb	-0.81	0.07	-0.20	0.12	0.26
V	-0.85	0.19	-0.16	0.05	0.30
Ba	-0.73	-0.14	-0.25	0.10	0.20
Na	-0.17	0.27	0.62	-0.07	-0.06
Mg	0.05	0.80	0.18	-0.05	-0.13
Al	-0.24	0.92	0.06	0.00	0.03
Si	-0.13	0.93	0.08	0.05	-0.02
P	-0.89	0.17	0.01	-0.05	-0.05
S	0.19	0.36	0.65	-0.04	-0.27
Cl	0.05	0.10	-0.03	0.90	0.01
K	-0.27	0.90	0.02	0.00	0.09
Ca	0.09	0.67	0.10	0.16	-0.24
Eigenvalue	7.51	4.84	1.55	1.39	1.11
Cumulative Eigenvalue	7.51	12.35	13.91	15.30	16.41
%Variance	32.66	21.05	6.76	6.05	4.83
% Cumulative Variance	32.66	53.70	60.64	66.51	71.34

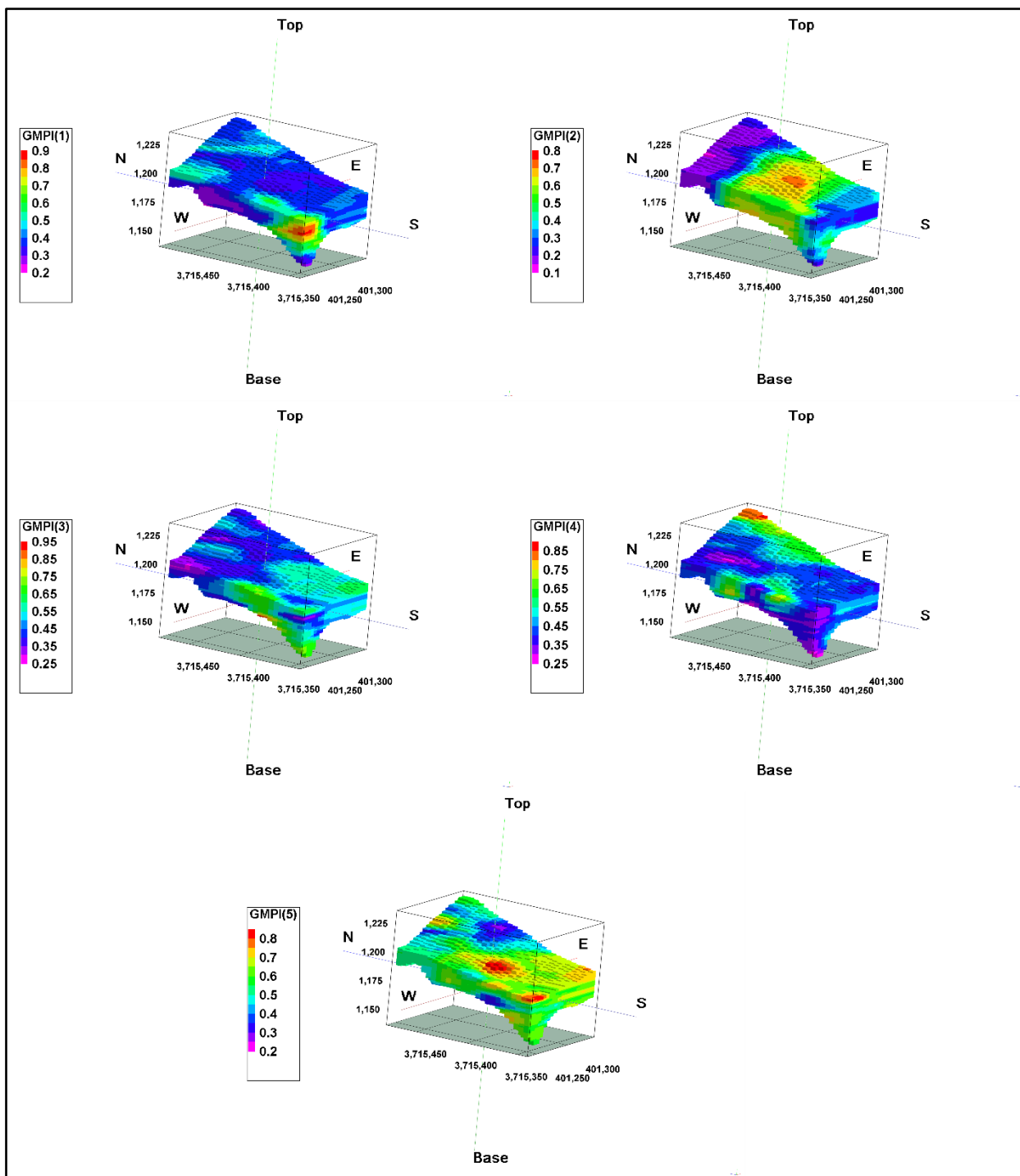


Figure 6. GMPI distribution map for Cr, Fe, Pb, Ti, Rb, V, Ba, P (GMPI1); Mg, Al, Si, K, Ca (GMPI2); Ta, Zn, Na, S (GMPI3); Cr, Cl (GMPI4); and Sr (GMPI5) indicator factors.

### 5.2. Halos index

It is likely that the significant Zn–Pb enrichments are found on the SW portion of the block near the fault-controlled shale contact, though the enrichment in Zn ores occurs both on the NE and SW of the block. Therefore, the ore is replaced epigenetically in hydrothermally altered shale as well as the faulted-fractured shale contact. It is interesting that the concentration of the elements

and ore values increase consistently toward the hydrothermally shale rocks with depth. The multiplicative composite rock-geochemical halos of multi-element data have been successfully used to delineate the possible exploration target for concealed mineralization [29]. Primary halo zoning can help to assess the level of the erosion and the extension of the supra-ore halos from sub-ore halos. For this purpose, theratios of

anomalous geochemical halos of ore elements were applied for the zonality of Pb-Zn sulfide mineralization. In order to calculate the composite halos, the anomalous values of Ba/Zn, Mn/(Pb+Zn), Cu/(Pb+Zn)(Ba.Mg)/(Pb.Zn), (Ba.Ca)/(Pb.Zn), (Ca.Mg)/(Pb.Zn), (Na.S)/(Pb.Zn), Ba/Sm, Pb/(Pb+Zn), Zn/(Pb+Zn), Zn/Pb, SiO<sub>2</sub>/Zn, Fe/(Fe+Pb+Zn), V/Cr, and V/(Ni+V) were determined. One of the most useful applications of the composite geochemical

halos is to find the location of blind ore [30]. After making vertical models of the halos, the mean values of each index were calculated for different levels from the surface toward the depth and plotted on a graph in Figure 7. Accordingly, Zn/(Pb+Zn), Zn/Pb, SiO<sub>2</sub>/Zn, and V/(Ni+V) of the composite halos demonstrate an increase above them in zone of the Haft-Savaran Pb-Zn mineralization in the SW to NE trend.

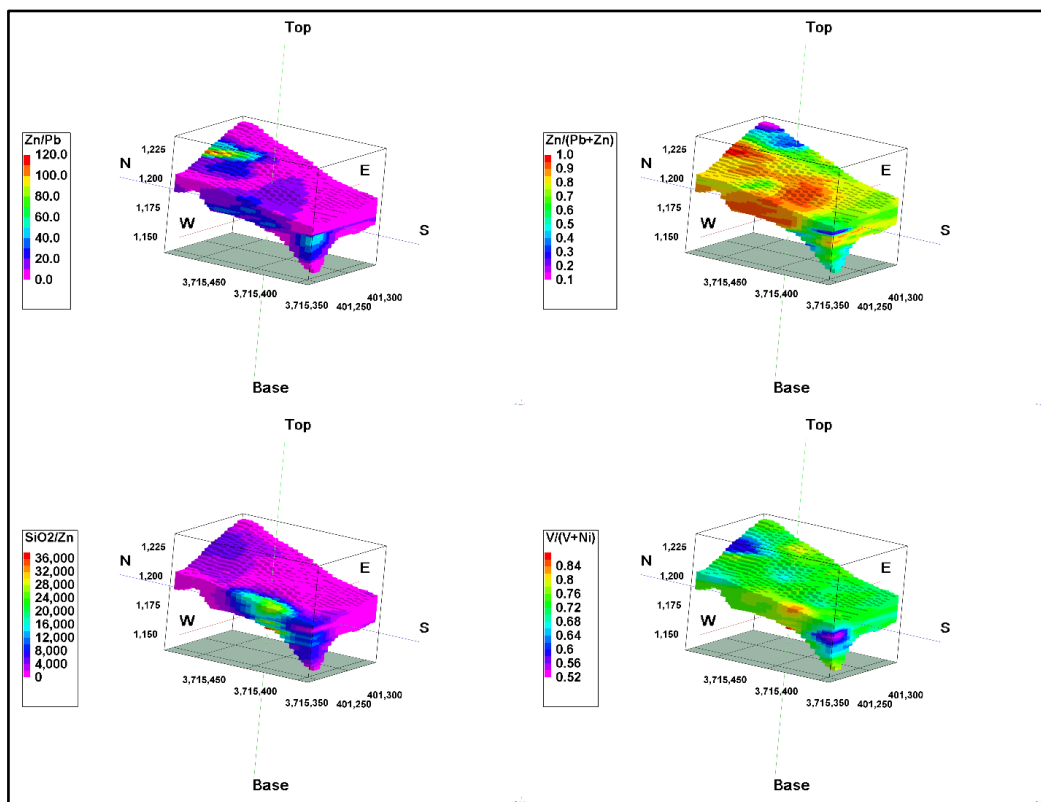


Figure 7. Multiplicative composite vertical litho-geochemical halos versus depth at Haft-Savaran mine based on Zn/(Pb+Zn), Zn/Pb, SiO<sub>2</sub>/Zn, and V/(Ni+V) contents.

### 5.3. Alteration index

The rocks of the area have hydrothermal alterations. Consequently, in order to find the relationships between mineralization and alteration in the area, many alteration indices were developed for the presence of alteration, and 3D alteration models were produced (Table). Sericitization index ( $K_2O/(Na_2O+CaO)$ ) was observed in two areas and with a trend from east to west (Figure 5). The index distribution 3D model of Spitz–Darling ( $Al_2O_3/Na_2O$  ratio) shows an enrichment of  $Al_2O_3$  rather than the  $Na_2O$  unit that refers to empty sodic in rocks of the region (Figure 5). High-grade area of this variable in the center and SW of the region is visible as small discrete areas. The index

distribution 3D model of Alkali had almost the opposite trend with a Sericitization index and increased with increasing the distance from Pb-Zn mineralization (Figure 5). The Hashimoto index distribution 3D model that shows input of K and Mg, and exit of Ca and Na confirms the possible locations specified by mineralization ( $(MgO+K_2O)/(MgO+K_2O+CaO+Na_2O)$ ). This index is widely spread in the east and west regions with the enrichment in the west, and indicates that there is a further potential of these areas for mineralization. The index distribution 3D model of Silicification has a high-grade area in the SW and central part of area (Figure 5).

**Table 2. Summary of alteration indices to test for presence of alteration.**

Alteration Index	Element Ratios	Alteration Process	Source
Sericite Index	$K_2O/(K_2O+Na_2O)$	replacement of feldspar by sericite	[31]
Silicification Index	$SiO_2/(SiO_2+Al_2O_3)$	Si enrichment or depletion relative to Al.	[32]
Spitz-Darling	$Al_2O_3/Na_2O$	sodium depletion ( $Al_2O_3$ conserved)	[33]
Alkali Index	$Na_2O + CaO/(Na_2O + CaO + K_2O)$	loss of CaO and $Na_2O$ by destruction feldspar	[34]
Hashimoto Index	$MgO + K_2O/(MgO + K_2O + CaO + Na_2O)$	addition of Mg and K as chlorite and sericite	[35]
		loss of CaO and $Na_2O$ by destruction feldspar	[36]

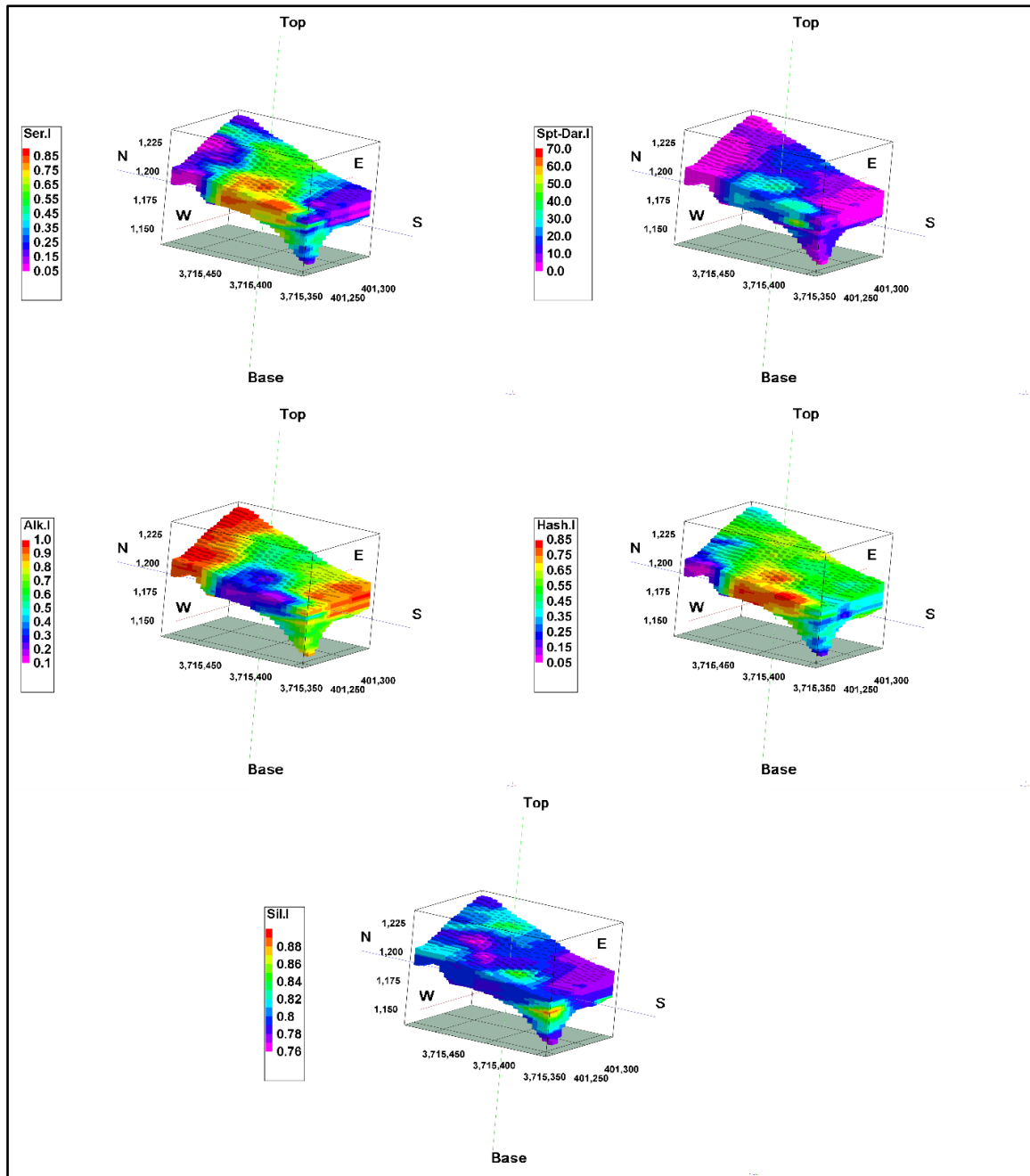


**Figure 8. Alteration models for Sericite Index(Ser.I), Spitz-Darling Index(Spt-Dar.I), Alkali Index(Alk.I), Hashimoto Index (Hash.I),and Silicification Index(Sil.I).**

The cluster analysis of halo index and alteration index presents three separate clusters of these indices (Figure 9). Cluster A contains the most metallic and non-metallic ratios with Pb and Zn in the region. Cluster B indicates indicators that are close to the silica and Alkali indices, and finally, cluster C indicates the mineralization of Zn and Pb in relation to the Hashimoto, Sericite, and Spitz-Darling indices.

In the next stage, the factor analysis was performed on the composite halo index and alteration index. After preparing and standardizing them, a three-stepwise factor analysis was used to infer the important indicators for mineralization. In the first stage, factor analysis clearly revealed 9 factors on the basis of the chemical indices of the samples. At this stage, the Ba/Zn, Mn/(Pb+Zn), Ba/S, and Fe/(Fe+Pb+Zn) indices were set aside due to the lower factor load factor. The remaining indicators were sent to the second stage of factor analysis. In the second stage, Cu/(Pb+Zn) and Fe/Zn were excluded from the calculations. The third stage and the last stage of factor analysis provided seven distinct and effective factors on the introduced indicators (Table 3). The specific

values for these factors are presented in Table 3. The first factor with a specific value of 5.04 and 25.21% variance includes Fe/(Pb+Zn), (Ca.Ba)/(Pb.Zn), (Ca.Mg)/(Pb.Zn), (Mn.Ba)/(Pb.Zn), and (Na.S)/(Pb.Zn), which are related to the trend of these indices in each borehole. The second factor with a specific value of 3.18 and 15.90% variance is the Hashimoto, Sericite, Spitz-Darling, and Alkali alteration indices. The Alkali index here is associated with a negative coefficient and the trend that increases out of the mineralization domain. Therefore, the existence of a negative affinity can be an exact calculation. The third factor with a specific value of 2.31 and 11.57% variance can be an indicator of Pb and Zn mineralization. The fourth factor with a specific value of 1.74 and 8.72% variance can be related to silica mineralization in the region, with silica associated with Pb and Zn anomalies. The existence of a silicon substitution index along with the indices (Si.K.Al)/(Pb.Zn) and the SiO<sub>2</sub>/(Pb+Zn) index are indicative of this. Due to the low variance and special value of other factors, they were not considered.

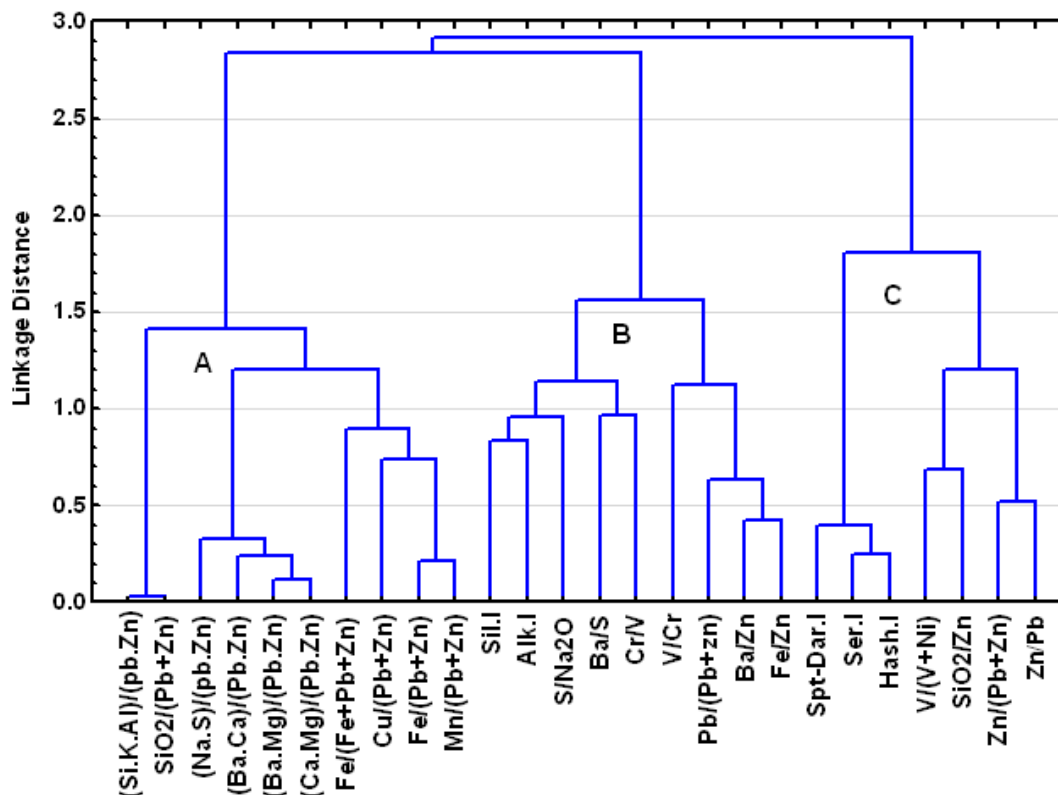


Figure 9. Cluster analysis of halo index and alteration index.

**Table 3. Third stage of stepwise factor analysis on geochemical indicators in Haft-Savarán area.**

Variables	Factor 1	Factor 2	Factor 3	Factor 4	Factor 5	Factor 6	Factor 7
Zn/Pb	-0.13	-0.08	0.74	0.05	0.05	0.12	-0.01
Pb/(Pb+Zn)	-0.13	-0.12	-0.93	0.00	0.02	0.16	-0.01
Zn/(Pb+Zn)	0.13	0.12	0.93	0.00	-0.02	-0.16	0.01
Fe/(Pb+Zn)	0.79	0.16	-0.10	0.07	-0.05	0.15	0.12
SiO <sub>2</sub> /Zn	-0.22	-0.05	0.05	0.05	0.04	-0.79	-0.09
SiO <sub>2</sub> /(Pb+Zn)	0.43	0.22	0.08	0.82	-0.03	0.02	0.13
(Ca.Mg)/(Pb.Zn)	0.93	0.09	0.02	0.09	0.06	0.00	-0.02
(Ba.Ca)/(Pb.Zn)	0.88	-0.02	0.08	0.19	0.02	0.00	-0.10
(Ba.Mg)/(Pb.Zn)	0.87	0.17	0.06	0.11	-0.03	0.01	0.05
(Si.K.Al)/(Pb.Zn)	0.33	0.10	0.08	0.87	-0.04	-0.01	0.12
(Na.S)/(Pb.Zn)	0.86	-0.08	0.03	-0.03	-0.03	-0.03	-0.05
V/Cr	0.02	0.05	0.04	-0.07	-0.88	0.19	0.03
V/(V+Ni)	0.14	0.23	0.10	-0.12	0.04	-0.78	0.02
Cr/V	0.00	0.13	0.04	-0.05	0.89	0.11	0.02
S/Na <sub>2</sub> O	0.02	0.01	-0.01	-0.01	0.01	-0.07	-0.96
Hash.I	0.00	0.87	0.01	0.04	0.01	-0.05	0.12
Ser.I	0.07	0.92	0.06	0.06	0.06	-0.08	-0.17
Spt.Dar.I	0.16	0.82	-0.05	-0.06	0.02	0.07	0.02
Alk.I	-0.04	-0.93	-0.14	-0.04	0.00	0.14	-0.04
Sil.I	-0.21	-0.22	-0.08	0.69	0.09	0.09	-0.26
Eigenvalue	5.04	3.18	2.31	1.74	1.62	1.26	1.01
Cumulative Eigenvalue	5.04	8.22	10.53	12.28	13.90	15.16	16.17
%Variance	25.21	15.90	11.57	8.72	8.09	6.32	5.03
% Cumulative Variance	25.21	41.11	52.67	61.40	69.48	75.80	80.84

## 6. Conclusions

By comparison of Pb-Zn and other element anomalies with alteration indices and alteration halos, it was determined that mineralization occurred in the alteration zones. The development of alteration indices is an evidence of the direction of mineralization solutions along the NE-SW trend, and this trend is in accordance with the fault in the region. The significant adaptation of alteration indicators and metal anomalies show that alteration indicators can be used to detect mineralization. According to the existence potential for Pb-Zn mineralization in the Malayer-Isfahan metallogenic zone, the results of this research work can be used in future exploration works in the region, especially for the areas in the regional exploration and polymetal mineralization.

## References

- [1]. Ghorbani, M. (2002). An introduction to economic geology of Iran. National Geoscience Database Iran. Report 2. 695 P. (In Persian).
- [2]. Gilg, H.A., Boni, M., Balassone, G., Allen, C.R., Banks, D. and Moore, F. (2006). Marble hosted sulfide ores in the Angouran Zn-(Pb-Ag) deposit, NW Iran: interaction of sedimentary brines with a metamorphic core complex. *Miner Deposita*. 41: 1-16.
- [3]. Taylor, R.D., Leach, D.L., Bradley, D.C. and Pisarevsky, S.A. (2009). Compilation of Mineral Resource Data for Mississippi Valley-Type and Clastic-Dominated Sediment-Hosted Lead-Zinc Deposits. U.S. Geol Surv Open-File Rep 2009-1297. 42 P.
- [4]. Ghorbani, M., Tajbakhsh, P. and Khoie, N. (2000). Lead and Zinc Deposits in Iran. GSI Book. No. 75. 512 P.
- [5]. Dixon, C.J. and Pereira, J. (1974). Plate tectonics and mineralization in the Tethyan Region. *Mineralium Deposita*. 9: 185-198.
- [6]. Reichert, J. (2007). A metallogenic model for carbonate-hosted non-sulphide zinc deposits based on observations of Mehdi Abad and Irankuh, Central and Southwestern Iran. Ph.D. Thesis. Martin Luther University. Halle Wittenberg.
- [7]. Rajabi, A., Rastad, E. and Canet, C. (2013). Metallogeny of Permian-Triassic carbonate-hosted Zn-Pb and F deposits of Iran: a review for future mineral exploration. *Australian Journal Earth Science*. 60: 197-216.
- [8]. Rajabi, A., Rastad, E., Alfonso, P. and Canet, C. (2012). Geology, ore facies and sulfur isotopes of the Koushk vent-proximal sedimentary-exhalative deposit, Posht-e-Badam block, Central Iran. *International Geology Review*. 54: 1635-1648.

- [9]. Wang, C.M., Carranza, E.J.M., Zhang, S.T., Zhang, J., Liu, X.J., Zhang, D., Sun, X. and Duan, C.J. (2013). Characterization of primary geochemical haloes for gold exploration at the Huangxiangwa gold deposit, China. *Journal of Geochemical Exploration*. 124: 40-58.
- [10]. Hosseini-Dinani, H., Aftabi, A., Esmaeili, A. and Rabbani, M. (2015). Composite soil-geochemical halos delineating carbonate-hosted zinc-lead-barium mineralization in the Irankuh district, Isfahan, west-central Iran. *Journal of Geochemical Exploration*. 156: 114-130.
- [11]. Run-Sheng, H., Jin, C.H., Feng, W., Xue-Kun, W. and Yuan, L. (2015). Analysis of metal-element association halos within fault zones for the exploration of concealed ore-bodies- A case study of the Qilinchang Zn-Pb-(Ag-Ge) deposit in the Huize mine district, northeastern Yunnan, China. *Journal of Geochemical Exploration*. 159: 62-78.
- [12]. Carranza, E.J.M. and Sadaghi M. (2012). Primary geochemical characteristics of mineral deposits- Implications for exploration. *Ore Geology Reviews*. 45: 1-4.
- [13]. Hosseini-Dinani, H. and Aftabi, A. (2016). Vertical litho-geochemical halos and zoning vectors at Goushfil Zn-Pb deposit, Irankuh district, southwestern Isfahan, Iran: Implications for concealed ore exploration and genetic models. *Ore Geology Reviews*. 72: 1004-1021.
- [14]. Li, Y., Zhang, D., Dai, L., Wan, G. and Hou, B. (2016). Characteristics of structurally superimposed geochemical haloes at the polymetallic Xiasai silver-lead-zinc ore deposit in Sichuan Province, SW China. *Journal of Geochemical Exploration*. 169: 100-122.
- [15]. Harris, J.R., Wilkinson, L. and Grunsky, E.C. (2000). Effective use and interpretation of litho-geochemical data in regional mineral exploration programs: application of Geographic Information Systems GIS technology. *Ore Geology Review*. 16: 107-114.
- [16]. Hannington, M.D., Santaguida, F., Kjarsgaard, I.M. and Cathles, L.M. (2003). Regional-scale hydrothermal alteration in the Central Blake River Group, western Abitibi sub-province, Canada: implications for VMS prospectivity. *Mineralium Deposita*. 38: 393-422.
- [17]. Sillitoe, R.H. (1995). Exploration and discovery of base- and precious-metal deposits in the circum-Pacific region during the last 25 years (No. 19). *Society of Resource Geology*.
- [18]. Zandy, N. (2016). Determine the geochemical halos associated with Pb-Zn mineralization based on a combination of geochemical data mining and geological model in Khomein, Degree of Master of Science (M.Sc.) in mining Engineering, exploration. Arak University of Technology (In Persian).
- [19]. Mahmoudi, P., Rastad, E., Rajabi, A.R. and Pirnajmodine, H. (2014). Clastic-hosted Ore facies of the Haft Savaran Zn-Pb ore deposit, in South of Arak basin. 33Sumposium earth-science. (In Persian).
- [20]. Lepeltier., C. (1969). A simplified statistical treatment of geochemical data by graphical representation. *Economic Geology*. 64 (5): 538-550.
- [21]. Panahi, A., Cheng, Q. and Bonham-Carter, F. (2004). Modelling lake sediment geochemical distribution using principal component, indicator kriging and multifractal power-spectrum analysis: a case study from Gowganda, Ontario. *Geochemistry: Exploration, Environment, Analysis*. 4: 59-70.
- [22]. Yousefi, M., Kamkar-Rouhani, A. and Carranza, E.J.M. (2012). Geochemical mineralization probability index (GMPI): A new approach to generate enhanced stream sediment geochemical evidential map for increasing probability of success in mineral potential mapping. *Journal of Geochemical Exploration*. 115: 24-35.
- [23]. Cheng, Q., Bonham-Carter, G.F., Wang, W., Zhang, S., Li, W. and Xia, Q. (2011). A spatially weighted principal component analysis for multi-element geochemical data for mapping locations of felsic intrusions in the Gejiu mineral district of Yunnan, China. *Computers and Geosciences*. 5: 662-669.
- [24]. Zuo, R. (2011). Identifying geochemical anomalies associated with Cu and Pb-Zn skarn mineralization using principal component analysis and spectrum-area fractal modeling in the Gandese Belt, Tibet (China). *Journal of Geochemical Exploration*. 111: 13-22.
- [25]. Yousefi, M., Carranza, E.J.M. and Kamkar-Rouhani, A. (2013). Weighted drainage catchment basin mapping of geochemical anomalies using stream sediment data for mineral potential modeling. *Journal of Geochemical Exploration*. 128: 88-96.
- [26]. Zuo, R., Cheng, Q. and Agterberg, F.P. (2009). Application of a hybrid method combining multilevel fuzzy comprehensive evaluation with asymmetric fuzzy relation analysis to mapping prospectivity. *Ore Geology Reviews*. 35: 101-108.
- [27]. Yousefi, M., Kamkar-Rouhani, A. and Carranza, E.J.M. (2014). Application of staged factor analysis and logistic function to create a fuzzy stream sediment geochemical evidence layer for mineral prospectivity mapping. *Geochemistry: Exploration, Environment, Analysis*. 14 (1): 45-58.
- [28]. Yousefi, M. and Carranza, E.J.M. (2014). Fuzzification of continuous-value spatial evidence for mineral prospectivity mapping. *Computer and Geoscience*. 74: 97-109.
- [29]. Aung, P.W.A. and Van Moort, J.C. (1995). Litho-geochemistry and electron paramagnetic

resonance (EPR) of rocks in the Hercules mine area- exploration and alteration studies Geology Department. University of Tasmania. Unpublished report to Pasmaenco Exploration. Bumie. 50 P.

[30]. Govett, G.J.S. (1983). Rock geochemistry in mineral exploration: Handbook of Exploration Geochemistry 3. Elsevier. Amsterdam. 461 P.

[31]. Spitz, G. and Darling, R. (1978). Major and minor element lithogeochemical anomalies surrounding the Louvem copper deposit, Val D'Or, Québec. Canadian Journal of Earth Sciences. 15 (7): 1161-1169.

[32]. Saeki, Y. and Date, J. (1980). Computer application to the alteration data of the footwall dacite lava at the Ezuri Kuroko deposits, Akita prefecture. Mining Geology. 30 (162): 241-250.

[33]. Van Ruitenbeek, F.J., Cudahy, T., Hale, M. and van der Meer, F.D. (2005). Tracing fluid pathways in

fossil hydrothermal systems with near-infrared spectroscopy. Geology. 33 (7): 597-600.

[34]. Ishikawa, Y., Sawaguchi, T., Iwaya, S. and Horiuchi, M. (1976). Delineation of prospecting targets for Kuroko deposits based on models of volcanism of underlying dacite and alteration halos. Mining Geology. 26: 105-117.

[35]. Date, J., Watanabe, Y. and Saeki, Y. (1983). Zonal alteration around the Fukazawa Kuroko deposits, Akita Prefecture, Northern Japan, in Ohmoto, H. and Skinner, B.J., eds., Kuroko and related volcanogenic massive sulphide deposits. Economic Geology Monograph. 5: 507-522.

[36]. Goodfellow, W.D., Lydon, J.W. and Turner, R.J.W. (1993). Geology and genesis of stratiform sediment-hosted (SEDEX) zinc-lead-silver sulphide deposits. Mineral Deposit Modeling: Geological Association of Canada. Special Paper. 40: 201-251.

## Appendix1

**Statistical parameters of main element concentrations of samples from Haft-Savaran area.**

Variable	Mean	Median	Minimum	Maximum	Standard deviation	Skewness	Kurtosis
Cr	87.21	90	7.50	213	34.65	0.59	1.70
Cu	61.96	40	10	201	55.43	1.45	1.06
Fe	92943	71385	331	339723	68355	0.97	0.58
Mn	7298	3595	103	38061	8521	1.57	1.78
Ni	42.87	40	7.50	96	14.60	0.33	1.56
Pb	2405	560	20	10943	3409	1.48	0.92
Sr	82.65	70	20	228	46.56	1.38	1.68
Ta	74.39	70	7.50	147	24.62	1.59	2.37
Zn	4065	1635	103	12996	4670	1.080	-0.43
Zr	201	200	7.50	460	71.53	0.06	0.88
Ti	3688	3911	735	5546	1153	-0.64	-0.34
Rb	97.82	100	7.50	180	38.62	-0.49	-0.24
V	113	115	20	190	35.99	-0.26	-0.58
Ba	223	220	7.50	530	107	0.22	-0.01

## کاربرد شاخص آلتراسیون برای اکتشاف سرب و روی منطقه هفت سواران خمین

نسترن زندی ایلقانی<sup>۱</sup>، فریدون قدیمی<sup>۱\*</sup> و محمد قمی<sup>۲</sup>

۱- دانشکده مهندسی معدن، دانشگاه صنعتی اراک، اراک، ایران

۲- دانشکده مهندسی معدن و متالورژی، دانشگاه صنعتی امیرکبیر، ایران

ارسال ۲۰۱۷/۸/۱۶، پذیرش ۲۰۱۷/۱۰/۲۵

\* نویسنده مسئول مکاتبات: ghadimi@arakut.ac.ir

---

### چکیده:

منطقه کانی‌سازی سرب و روی هفت سواران با سن ژوراسیک زیرین در بخش جنوبی اراک و در کمربند متالوژنیک ملایر- اصفهان واقع شده است. ماسه‌سنگ و شیل ژوراسیک زیرین مهم‌ترین سنگ‌های میزبان سرب و روی منطقه هستند. در منطقه هفت سواران ۱۷۰ نمونه از ۳۳ چاه حفاری برداشت و ۴۴ عنصر به روش ICP-MS اندازه‌گیری شد. کانی‌سازی سرب و روی به توسط شاخص آلتراسیون و اندیس‌هایی چون سریسیتی شدن، اسپیتز- دارلینگ، آکالی، هاشیمیتو و سیلیسی شدن مورد بررسی قرار گرفت. این بررسی نشان داد شاخص‌های سریسیتی، اسپیتز- دارلینگ، هاشیمیتو و سیلیسی شدن در اطراف کانی‌سازی افزایش و شاخص آکالی کاهش می‌یابد. روند شاخص‌های آلتراسیون هم‌جهت با محلول کانی‌سازی و در جهت شمال شرق- جنوب غرب است و این روند منطبق با گسل‌های منطقه است. با توجه به نمودارهای سه‌بعدی و سایر اطلاعات مشخص شد که عناصر سرب و روی و هم‌چنین آهن، منگنز، کروم و نیکل در منطقه آلتراسیون ته‌نشست یافته‌اند.

**کلمات کلیدی:** هاله آلتراسیون، شاخص آلتراسیون، کانی‌سازی سرب و روی، هفت سواران.

---